New monitoring method to characterize individual modules in large photovoltaic systems

Eneko Ortega*, Gerardo Aranguren, Juan Carlos Jimeno

Technological Institute of Microelectronics, University of the Basque Country (UPV/EHU), 48013 Bilbao, Spain

ARTICLE INFO

ABSTRACT

Photovoltaic (PV) systems power losses are approximately 15–20% of the performance ratio for current PV systems. There are several reasons that explain PV modules failures, and since they are connected in series to the rest of the string, a failure in one module may result in losses in the entire string. In addition, some of these failures, if are not fixed in time may become permanent and may reduce the lifespan of the PV modules. Periodic monitoring is the only way to detect these failures. Monitoring techniques oriented to groups of modules are unable to detect faults in individual modules. I-V curve tracers, which are oriented to module level and use power electronics components and large capacitors, require to disconnect the PV module from the rest of the system and long measurement times. This works proposes a methodology, that is able to take partial measurements of individual PV modules and recompose their characteristics with only small capacitors in the range of tens of microfarads and without power electronics components. The monitoring methodology is able to measure individual PV modules without modifying the electrical interconnection circuit and to deviate the operating point to ±0.3 A and 5 V in less than 5 ms. From this deviation, the system recomposes the PV module I-V characteristics with accuracies that are between 1 and 3% for the region close to maximum power.

1. Introduction

Solar photovoltaic (PV) energy source is the renewable energy source that has increased the most during the past decades. The installed solar PV capacity is increasing almost exponentially, by more than 30% each year (Sawin et al., 2017). In 2018, more than 100 GW of new PV capacity was installed (Jäger-Waldau, 2019). In addition, large systems with hundreds of thousands of PV modules are increasingly common. PV systems performance is usually evaluated in terms of the performance ratio (PR) (Blaesser, 1997). Unfortunately, for current PV systems, power losses are approximately 15–20% of the PR (Kumar and Sudhakar, 2015; Khalid et al., 2016; Matsumoto et al., 2016). Failures in PV module are behind a significant part of PR losses.

Failures in PV modules may be caused by several reasons such as corrosion failures (Cristaldi et al., 2015), cell cracks (Köntges et al., 2010; Kajari-Schršder et al., 2012; Morlier et al., 2015), hot-spots (Kim and Krein, 2013; García et al., 2014), encapsulation failures (Park et al., 2013), electrical or mechanical interconnection failures (Cristaldi et al., 2015), potential induced degradation (Hoffmann and Koehl, 2014), accumulation of dust or soiling (Caron and Littmann, 2013; Cova et al., 2018) or partial shadows (Mäki and Valkealahti, 2012) among others. Since PV modules are connected in series to the rest of the string, the

failure of a single PV module may cause power looses in the whole string. Furthermore, some of these failures, if not fixed in time, can become permanent and accelerate the degradation of PV modules. Periodic monitoring is the only way to detect failures in a PV system. Thus, many PV systems monitoring methods, which monitor the PV system at module level or measure groups of modules have been proposed, but there is no agreement regarding the appropriate level for monitoring the system (Ortega et al., 2017; Jones et al., 2018).

Some methods, based on several approaches, monitor the PV system at string, array or inverter level. These monitoring techniques usually combine a model of the PV system with temperature, irradiance and electrical output data. Operating conditions can be measured using either satellite data (Drews et al., 2007) or by adding temperature and irradiance sensors (Firth et al., 2010; Chouder and Silvestre, 2010; Silvestre et al., 2016; Mallor et al., 2017). Other methods use statistical analysis and machine learning techniques to evaluate data from the PV system to estimate the deviation from the optimum point (Vergura et al., 2009; Dhimish and Holmes, 2016; Belaout et al., 2018; Wang et al., 2018). Monitoring techniques oriented to groups of modules are able to detect significant energy losses, but are unable to detect faults affecting a single module or a small group of modules. In fact, monitoring at system level provides little information about individual

---

modules degradation or abnormal operating conditions (Jones et al., 2018). In addition, with system-level monitoring, even if a fault is detected, it is not clear which specific module is failing.

Methods for monitoring at module level can obtain several parameters from individual modules. Various technologies such as SunSniffer (Kilper et al., 2015), which measures PV modules voltage and temperature, and power optimizers such as SolarEdge or Tigo, which measure modules output and combine it with maximum power point tracking methods, have been introduced in the past. However, power optimizers handle the total power of PV modules, which makes them expensive solutions because they require power electronics. Module level monitoring methods can be classified in function of the number of parameters that are measured. When only module voltage is measured (Kilper et al., 2015; Teubner et al., 2017), it is possible to assess power losses, unless the fault is limiting the current of the string. If the current is also measured, the working point is known and thus it is possible to determine the module power losses (Fuentes et al., 2014; Han et al., 2015; Samara and Natsheh, 2019). However, by only measuring these two parameters, it cannot be known whether the power loss is caused by a failure in the module or in the rest of the system and the power loss is due to a module mismatch. If two more parameters, current and voltage variations, i.e., the current–voltage (I-V) characteristics of the PV module, are added, the module is electrically characterized and in this way, the power loss origin can be determined.

I-V curve tracers measure the I-V characteristics of PV modules or arrays by measuring a set of operating points that are defined by a value of current and voltage, from short-circuit to open-circuit. Many methods have been suggested to measure the I-V characteristic of PV modules, strings or arrays based on different types of variable loads. Approaches based on resistive loads (Van Dyk et al., 2005; Ibrahim, 2011; Rivai and Rahim, 2014), connect a plethora of resistances to the module, limiting its output current at several values and measuring their corresponding point on the I-V curve. These methods are limited by the power dissipated by the resistance. When DC-DC converters are used (Enrique et al., 2005; Duran et al., 2007; Riley and Tolbert, 2015; Khatib et al., 2017), the PV module is connected to the input of the converter and a resistive load is connected to the output. By modifying the voltage of the converter, it is possible to modify the output power of the module and obtain the I-V curve by repeating this process several times. With the same methodology, other authors have proposed different combinations of transistors using MOSFET (Kuai and Yuvarajan, 2006; Belmili et al., 2010), BJT (Forero et al., 2006) or IGBT (Sahbel et al., 2013) transistors. Similarly, I-V curve tracers based on capacitive load move the operation point of the module with the charge of a variable number of capacitors controlled with several switches (Mahmoud, 2006; Muñoz and Lorenzo, 2006; Spertino et al., 2015; Erkaya et al., 2016). These methods are able to measure the full I-V characteristics of PV modules, typically in combination with temperature and irradiance data. However, most of these methods have three main limitations. First, since the entire I-V curve is measured, the monitoring system works at the module power. Therefore, power electronics components and capacitors on the order of tens of milli-farads are required. As a result, the cost and power consumption of I-V curve tracers are increased. Second, prior to measuring the PV module, these methods require disconnecting the PV module from the rest of the system at least 5 min before starting the measurements (Muñoz and Lorenzo, 2006), with subsequent power losses (Stein et al., 2014). Third, these techniques require relatively long measuring periods with stable operating conditions to obtain the full I-V curve, especially for modules with large response times.

Measuring the I-V curve of PV modules is an extended method for PV modules characterization and for fault and anomaly detection. However, previous limitations make I-V curve tracers unfeasible solutions for the automatic and continuous monitoring of large PV systems. This work proposes a new methodology that is able to take partial measurements of individual PV modules and recompose their
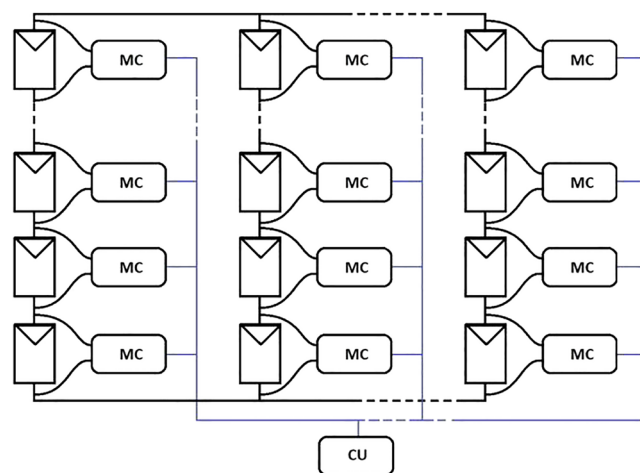

Fig. 1. Proposed monitoring methodology for an entire PV system. One monitoring circuit (MC) for each PV module and a control unit (CU) for the entire system.

characteristics with only small capacitors in the range of tens of microfarads and without power electronics components. Since the electronic circuit does not use power electronics components, the cost of the monitoring system is reduced from a few tens of dollars in an initial phase to a cost in the dollar range for large scale production with a high integration level. Except for the two capacitors, all the components could be included on a single integrated circuit for large scale production.

2. Description of the system

The proposed monitoring system includes a small electronic circuit called monitoring circuit (MC) for each PV module and a control unit (CU) for the entire PV system. The preliminary concepts of the monitoring methodology were introduced in (Ulasenka et al., 2015; Ortega et al., 2016; Ortega et al., 2018). The MC is connected in parallel to each PV module as shown in Fig. 1. As a consequence, the monitoring system does not interfere with the operation of the PV modules, and in the case of failure, it does not affect the PV system operation. Through power line communications (PLC) the CU would be connected to every MC in the PV system and controls the entire monitoring system without adding additional wires. From the CU, each individual PV module can be measured by ordering its MC to measure the module and send the measurement data. In the CU, the data are processed and visualized through a graphical interface. The CU is a complex system, but a single unit can monitor hundreds or thousands of modules. The proposed methodology is intended for central inverter systems, for which the information of each PV module is minimum and the usefulness of the monitoring system could be maximum. However, this methodology could be used with any system architecture.

Fig. 2 shows the simplified scheme of the MC. In the figure, there is only one MC connected to the middle module, but in a field application of the monitoring system, one MC is connected to each PV module of the system. The MC is a capacitive load based electronic circuit capable of producing and measuring small and quick variations in the working point of the PV module by using only low power components. The MC, which is powered by the PV module, is based on two small 22 µF tantalum capacitors and controlled by six switches. Two switches (diodes) are controlled only by the current direction, and four switches (transistors: SW1, SW2, Q1 and Q2) are controlled by a low-cost 8 bit PIC microcontroller (MCU in Fig. 2).

The MC has four operating modes as depicted in Fig. 3: standby (the initial state) and a three step monitoring sequence, called T1, T2 and T3. During the standby mode SW1 and SW2 are in the "b" position, as
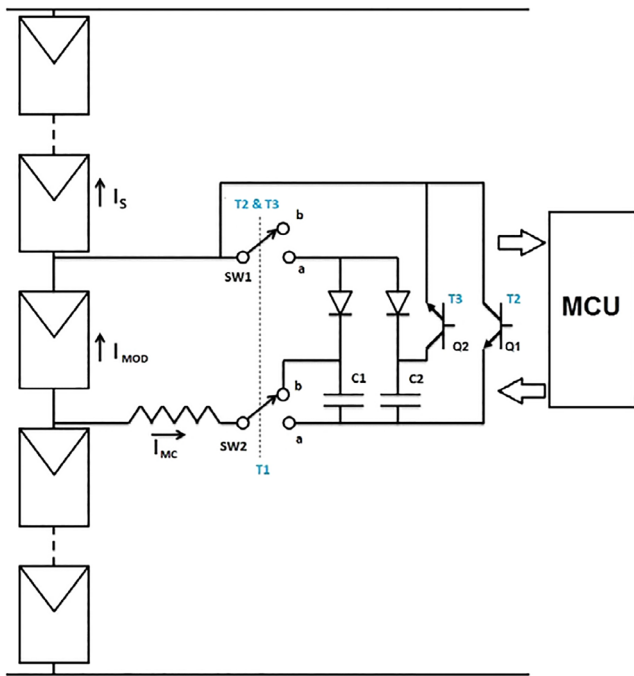
Fig. 2. MC simplified scheme connected to a PV module on a string. The circuit is based on 2 capacitors (C1 and C2), 6 switches, including: two diodes and four transistors (SW1, SW2, Q1 and Q2), and an 8 bit microcontroller (MCU). The blue T1, T2 and T3 labels indicate the step in which the switches are in active mode. (For interpretation of the references to colour in this figure legend, the reader is referred to the web version of this article.)

Fig. 4. Displacement of the operating point to short-circuit and open-circuit during T2 and T3 steps of the monitoring sequence with the MC.

showed in Fig. 2 and transistors Q1 and Q2 are in cut-off mode. In this mode no current is extracted from the PV module. When the CU orders to measure the PV module, the MC wakes up, and the monitoring sequence is performed as indicated in Fig. 3.

In the first step, T1, SW1 and SW2 are switched to the "a" position and Q1 and Q2 remain in the cut-off position. During this step, C1 and C2 are charged to the operating voltage of the module by the diodes. Through additional circuitry, that is not depicted in the figure, this process is performed slowly, draining only a small amount of current from the PV module.

During the second step, T2, SW1 and SW2 are switched again to the "b" position, Q1 is turned on to the active position and Q2 remains in cut-off mode. In Fig. 2, this step is depicted with T2 in the "b" position of the switches and in the active transistor, Q1. During this step, the circuit discharges C1 towards the PV module with a current limited to 0.3 A by additional circuitry. The electronic circuit tends to a new equilibrium situation in which capacitor C1 is charged to the inverted module voltage. Notice that in T2 the situation of C1 is inverted with regard to T1. The evolution of the PV module operating point is shown
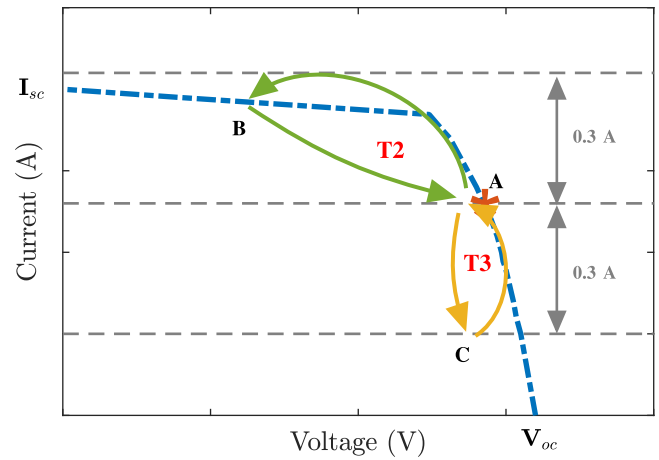
in Fig. 4 by the green colour. The connection of C1 to the module during T2 forces the operating point to follow the upper curve from point A to point B and to subsequently return back to point A.

During the last step, T3, SW1 and SW2 remain in the "b" position, Q1 returns to cut-off and Q2 turns on to active mode, as shown in Fig. 2 and depicted by T3. In this step, C1 and C2 are connected in series and their voltages are added. This step displaces the operating point to voltages higher than the operating voltage, with the same current limitation of 0.3 A as T2. In Fig. 4, the displacement of the operating point is shown in yellow. First, when capacitors C1 and C2 are discharged the operating point displaces from A to C and subsequently returns back to point A.

All the monitoring process is completed on the order of tens of milliseconds (<50 ms for the charging of the capacitors and <5 ms for the displacement of the PV module in both ways). The short times of the monitoring methodology enable the use of low power components, without power electronics, and small cross-section wires, thus avoiding thermal dissipation. Furthermore, short times ensure that operating conditions (irradiance and temperature) remain constant during the PV module characterization.

While the operating point of the PV module is being displaced in both directions (Fig. 4), the MCU takes several pairs of voltage and current values around the operating point, with 10 bits resolution and a 35 ms sampling period. The voltage is measured through a voltage divider and the current is measured from two ways. The absolute current is measured through a shunt connected in series to the PV string. Incremental currents are measured on higher resistances, connected to the MC but not to the string series. After the test, the measurement data are processed by the CU, which estimates the I-V curve and the maximum power of the PV module.
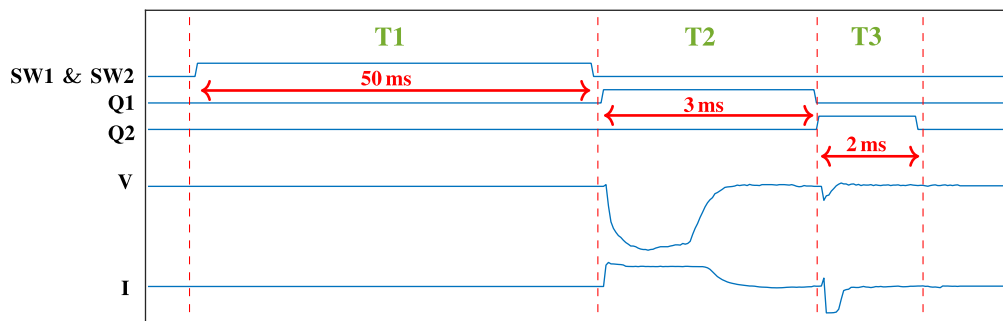

Fig. 3. Operating diagram of the MC. The MC has four states: Standby (the initial state) and T1, T2 and T3, the three steps of the monitoring sequence. The high value of the signal is associated with activation of the corresponding switches. Notice that signals are not on scale.
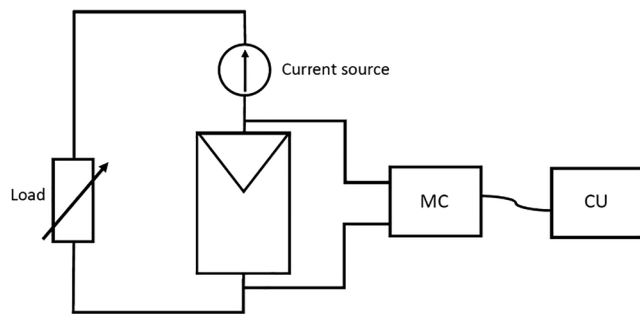
Fig. 5. Experimental test system scheme. PV module connected to a power supply and an electronic load. The MC is connected in parallel to the PV module, and the MC and the CU are connected through an isolated wired network.

3. Experimental test system

A reduced series of a prototype of the MC was designed and manufactured. The MC was evaluated using a 25 W Isofotón bifacial PV module. The PV module was illuminated with 18 lamps, which illumination level could be varied. This variability enabled the monitoring methodology to be tested under different illumination conditions to characterize the module in varying states.

Fig. 5 shows a simplified scheme of the test system used to evaluate the methodology, and Fig. 6 shows the experimental set-up. In the lower figure, the 25 W PV and the illumination system are shown. The PV module was connected in series (upper figure) to a power supply operating as the current source, which could vary from 0 to 5 A and 0 to 30 V. In addition, an electronic load was connected to them in series.
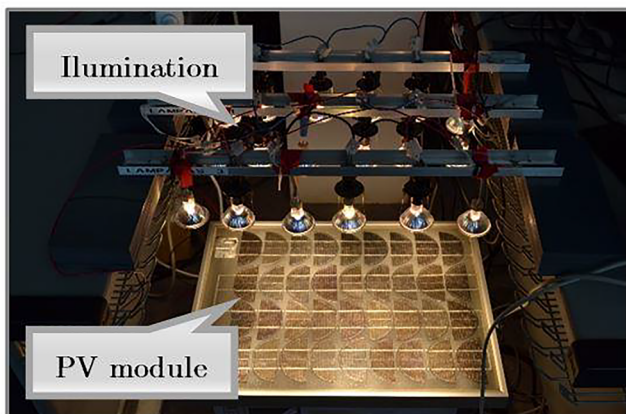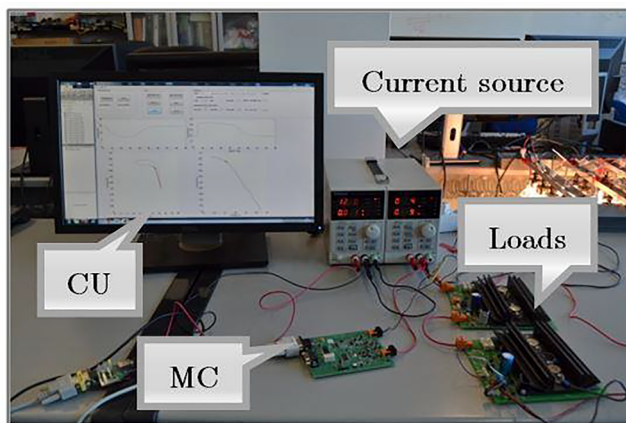

Fig. 6. Experimental set up. MC, CU, electronic loads and current source (top) and PV module and illumination (below).

The electronic load (formed by two individual loads) had a total voltage fixed at 26 V (13 V each). With the mounted test system, the operating point of the PV module could be adjusted by the current source.

The MC was connected in parallel to the PV module (Fig. 6) at the same points used to connect it with the current source and the load. The MC was, in turn, connected to the CU, which consists on a personal computer (PC) with a graphical user interface (GUI) developed in MATLAB (MathWorks Inc., Natick, MA, USA). The GUI receives the measurement data from the MC and processes them to obtain the I-V characteristic of the PV module around the operating point. All the results shown in this study were extracted from the GUI.

4. Dynamic I-V characteristic

To evaluate the concordance between the static PV module I-V characteristics and the dynamic data obtained from the MC system, the static I-V characteristics of the PV module were first measured without connecting the MC. For these experiments, the static characteristic had $V_{oc} = 15.15$ V and $I_{sc} = 0.45$ A. The operating point was fixed at $I_m = 0.19$A and $V_m = 14.9$ V and the MC was subsequently connected.

The measuring process begins with the load of the capacitors during the T1 step, as explained above. Then, in the T2 step, the PV modules operating point is shifted towards short-circuit. Fig. 7 shows the placement of the PV module under test in the string, where I_{mod} is the current of the PV module, I_s is the string current and I_{mc} is the current of the monitoring circuit. Any transient current in I_{mc} has a very small effect in the string current and forces the module current to move according to Eq. (1), which facilitates module current measurement.

$$I_{mod} = I_s - I_{mc} \tag{1}$$

As shown in Fig. 8 I_{mc} is a step-like function of approximately 0.3 A, which shifts the operating point 5 V towards short-circuit in approximately 0.25 ms (Section 1). The MC limits the current injected into the PV module, which remains at 0.3 A (Section 2) until the capacitor is discharged. Then, the output current starts to decrease more slowly (Section 3), and thus the PV module voltage starts to recover until it returns to the initial operating point. The entire sequence lasts less than 3 ms.

Fig. 9 shows the representation of these values against the static I-V characteristics. In Section 1, since the current variation is very fast, the dynamic I-V values are not able to follow the PV module I-V characteristics due to the intrinsic capacitance of the PV modules. When the operating point reaches the maximum deviation, it tends to the static I-
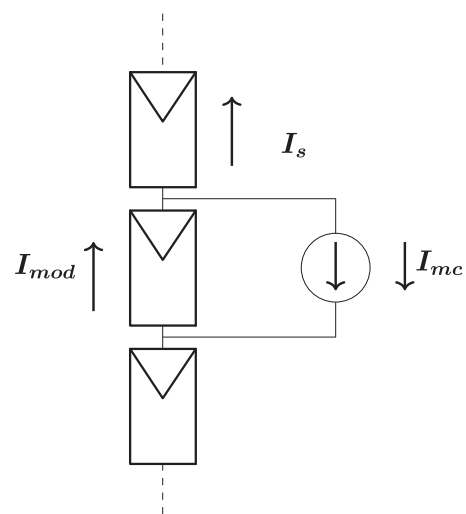

Fig. 7. Placement of the PV module under measure on the string. I_{mod} is the current of the PV module, I_s is the string current and I_{mc} is the current of the monitoring circuit.
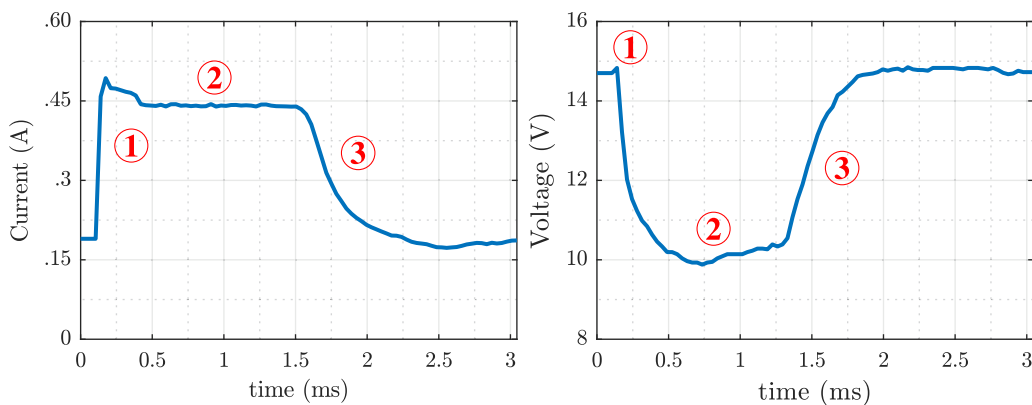
Fig. 8. Evolution of PV module current and voltage values during the T2 step of the monitoring sequence, displacing the operating point of the PV module towards short-circuit. Current (left) and voltage (right) of the PV module. Three sections are identified: Section 1 (shift of the operating point to short-circuit), Section 2 (discharge of the capacitor C1) and Section 3 (return to equilibrium).
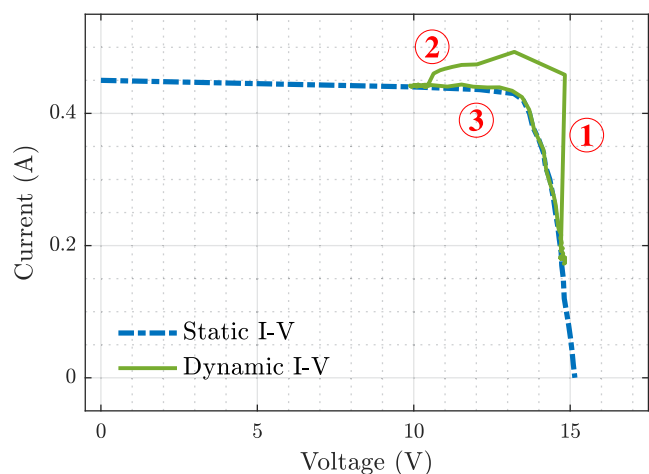

Fig. 9. Displacement of the operating point towards short-circuit during the T2 step of the monitoring sequence. Static I-V characteristics (dashed blue line) and dynamic I-V characteristics (green line). (For interpretation of the references to colour in this figure legend, the reader is referred to the web version of this article.)

Fig. 11. Displacement of the operating point towards open-circuit during step T3 of the monitoring sequence. Static I-V characteristics (dashed blue line) and dynamic I-V characteristics (yellow line). (For interpretation of the references to colour in this figure legend, the reader is referred to the web version of this article.)

V characteristics, with a current value close to I_{sc} (Section 2).The operating point stays there for 1 ms until the capacitor is discharged, and then, in Section 3, it returns to the initial operating conditions in a curve very close to the static I-V characteristics.

The third step, T3, in the measuring process consists of moving the operating point of the PV module to open-circuit. To that end, capacitors C1 and C2 decrease the output current of the module, as shown in Fig. 10, which shows the current and voltage values during this step. In Section 1, the MC displaces the operating point to the maximum deviation, which is a decrease of approximately 0.3 A. In Section 2 the current remains constant for 0.2 ms until C1 and C2 are discharged, and
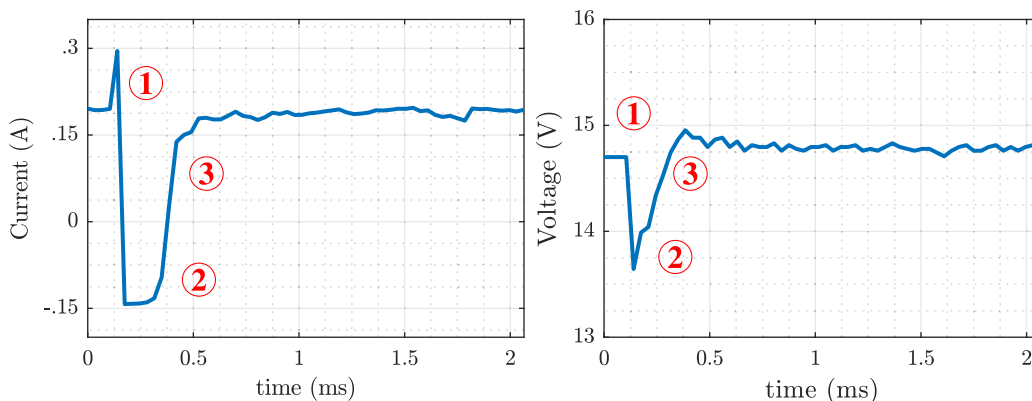
then, in Section 3, it returns to the initial operating point. As shown in Fig. 11, due to the intrinsic capacitance of the modules the dynamic I-V characteristics fits the static I-V characteristics only during Section 3, similarly to the second step.

5. Results discussion

Three different cases were analyzed. In one case the operating point of the PV module is at an intermediate current value (as in Section 4). The other two cases include more extreme conditions: one case with a higher current value and the other case with a lower current value.

Fig. 10. Evolution of PV module current and voltage values during step T3 of the monitoring sequence, which displaces the operating point of the PV module towards open-circuit. Current (left) and voltage (right) of the PV module. Three sections are identified: Section 1 (shift of the operating point to open-circuit), Section 2 (discharge of capacitors C1 and C2) and Section 3 (return to equilibrium).
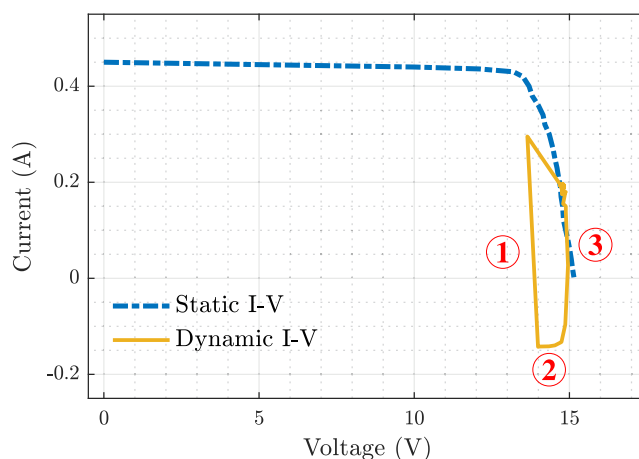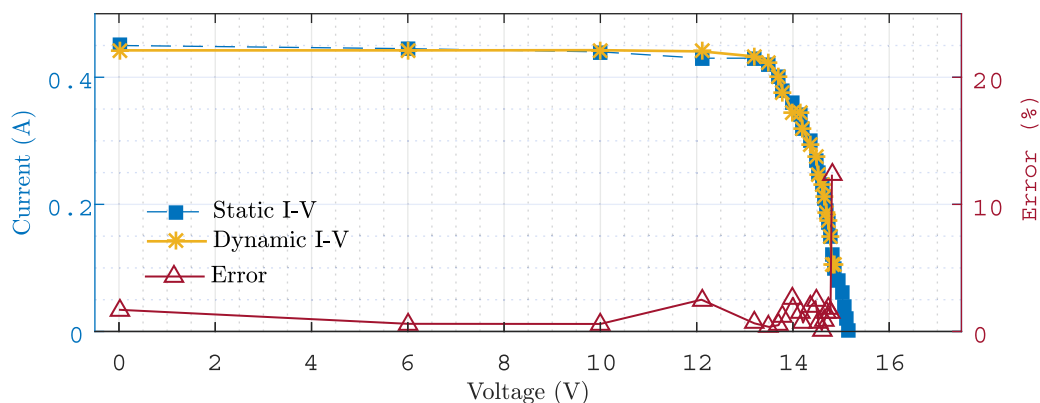
Fig. 12. Static (dashed blue) and dynamic (yellow) I-V characteristics and error rates (red) between them for intermediate current value operating point with $I_m = 0.19$A.

Figs. 9 and 11 show the dynamic evolution of the operating point for the intermediate current case, in which the PV module is working at 50% of the maximum power. A fast current evolution can be seen during Section 1 whereas in Section 2 the current value is sustained until the capacitor is discharged. Obviously, Sections 1 and 2 do not correspond with the static I-V curve of the PV module. Then, in Section 3 a slow charge is produced toward the static situation. Fig. 12 is obtained from these two figures and shows the dynamic I-V characteristics of the PV module, which correspond to Section 3 of the previous figures, plotted against the static I-V characteristic and the error rate between both measurements. The error rate was computed from raw measurements, without filtering or additional processing.

From the measurements it is possible to estimate the short-circuit current with an error rate below 3%. In the area around MPP, the error remains below 3% and for points closer to open-circuit, the error rate increases to above 10%. The error rate between the static maximum power (5.7 W) and the dynamic maximum power (5.8 W) was 1.8%.

For the high current values case, the operating point was fixed at $I_m = 0.28$ A and the dynamic I-V curve was obtained. Fig. 13 shows the static and dynamic I-V characteristics and the error rate between them. In this case, the short-circuit current is estimated with an error below 3%, but closer to open-circuit the error rate increases up to 10%. Around the maximum power the error rate between both curves was below 2.5% and the error rate to estimate the maximum power of the PV module (5.6 W) was 1.8%.

When the measurements were done closer to open-circuit, at the lower current value ($I_m = 0.09$ A) Fig. 14 was obtained. Close to open-circuit the error rate is below 5%. However, the error rate to estimate I_{sc} is above 15% and it remains in that range in the MPP area. Even with such low power, the maximum power (5.2 W) of the PV module can be estimated with an error of only 8.8%. This result is very noteworthy since the estimation was performed with the PV module working only at 24% of the nominal power of the PV module.

The proposed method is able to estimate the I-V characteristics of the PV module with 2 capacitors on the order of tens of microfarads, and the disturbance of the operating point lasts less than 5 ms. Of these 5 ms, only 0.875 ms (to short-circuit) and 0.35 ms (to open-circuit) are close to the I-V characteristics of the module. As shown in Fig. 12, the error remains below 3% for almost all of the I-V characteristics. The error only increases in function of the operating point for measurements closer to short-circuit when the operating point is in the vertical region of the I-V characteristics or closer to open-circuit, when the operating point is in the horizontal area.

To evaluate how the error rate differs in function of the capacitor size, the same experiment was repeated with two different capacitors, one capacitor of 11 µF and another of 242 µF. Table 1 shows the maximum displacements with errors below 3% for the three capacitors and the time required for each sequence. Fig. 15 shows the error for each capacitor along the static I-V characteristics. Capacitors on the order of tens or hundreds of microfarad induced a low error rate between the static and dynamic I-V characteristics, and it is possible to estimate I_{sc} with an error below 6%. However, capacitors on the order of hundreds of microfarads were discarded to avoid the use of electrolytic capacitors. With capacitors on the order of tens of microfarads, the error rate between the static and dynamic I-V characteristics is low enough to estimate the PV module I-V characteristic and the maximum power for current operating conditions. Conversely, if the PV system temperature and irradiance conditions during the test are known, it would be possible to calculate the expected I-V characteristics and the expected maximum power of the PV module from the reference PV module

Fig. 13. Static (dashed blue) and dynamic (yellow) I-V characteristics and error rates (red) between them for high current value operating point with $I_m = 0.28$ A. (For interpretation of the references to colour in this figure legend, the reader is referred to the web version of this article.)
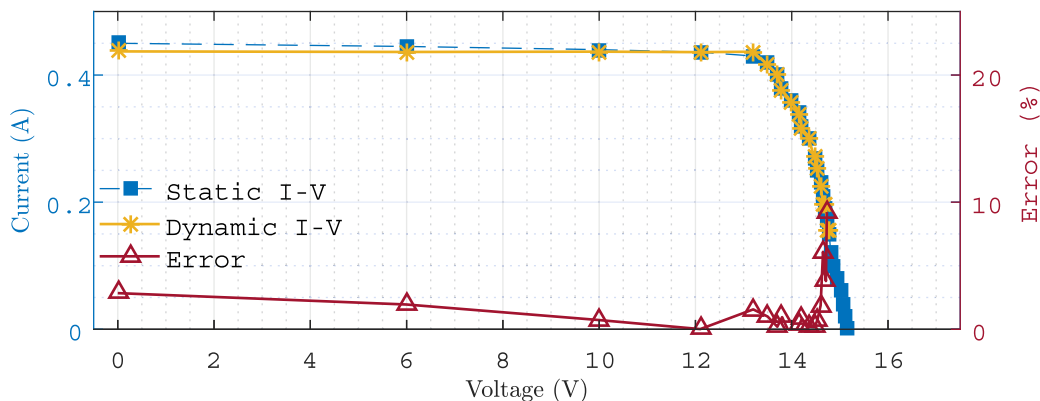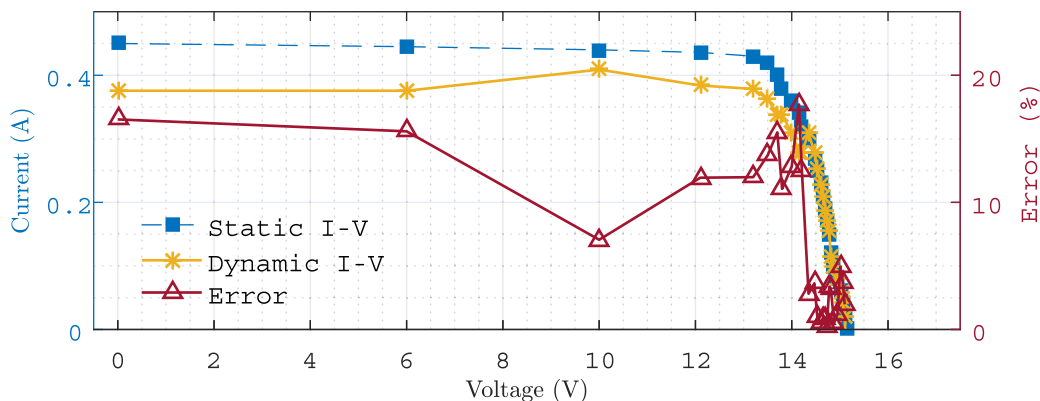
Fig. 14. Static (dashed blue) and dynamic (yellow) I-V characteristics and error rates (red) between them for low current value operating point with I_m = 0.09 A. (For interpretation of the references to colour in this figure legend, the reader is referred to the web version of this article.)

Table 1
Maximum and minimum voltage and current values, with the variations in brackets, during the experiment with an error below 3%, in function of the capacitor size. All the experiments were performed at an operating point with I_m = 0.19 A and V_m = 14.9 V.

	Operating point deviation					
	Deviation to short-circuit			Deviation to open-circuit		
	V_{min} (V)	I_{max} (A)	time (ms)	V_{max} (V)	I_{min} (A)	time (ms)
242 μF	10 (−5)	0.39 (+0.21)	11.3	14.9 (+0.3)	0.13 (−0.06)	4.2
22 μF	10 (−5)	0.39 (+0.21)	3.15	14.8 (+0.2)	0.16 (−0.03)	2.6
11 μF	12.0 (−3)	0.36 (+0.18)	2.9	14.7 (+0.1)	0.165 (−0.025)	1.9

parameters.

The monitoring methodology was also implemented in an outdoor 3.2 kW PV system consisting of 12 mono crystalline JINKO JKMS285-60 PV modules connected to an SMA Sunny Boy 3000TL-21 inverter. The monitoring process was performed on a single module without disconnecting it from the rest of the system. The MC proved to work reliably at the module voltage and current values and was able to disturb the 285 W PV modules to obtain a dynamic I-V curve equivalent to the curves obtained with the 25 W PV module, as shown in Fig. 16.

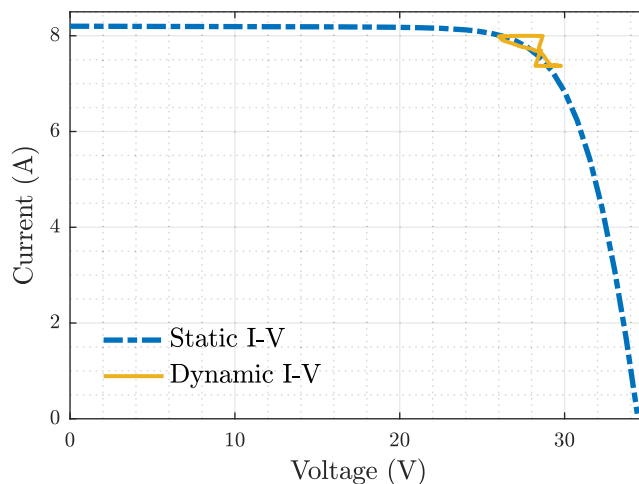However, from these data the estimation of the I-V curve is not

Fig. 16. Measurement with the MC in a Jinko JKMS285-60 PV module. Static I-V characteristics (dashed blue line) and dynamic I-V characteristics (yellow line). (For interpretation of the references to colour in this figure legend, the reader is referred to the web version of this article.)

immediate, since several factors such as the dependence on the set-up, the interactions with the rest of the system or the dynamic response of the PV modules must be considered. Thus, further processing is required to fit the dynamic I-V characteristics with the static characteristics of the PV module.
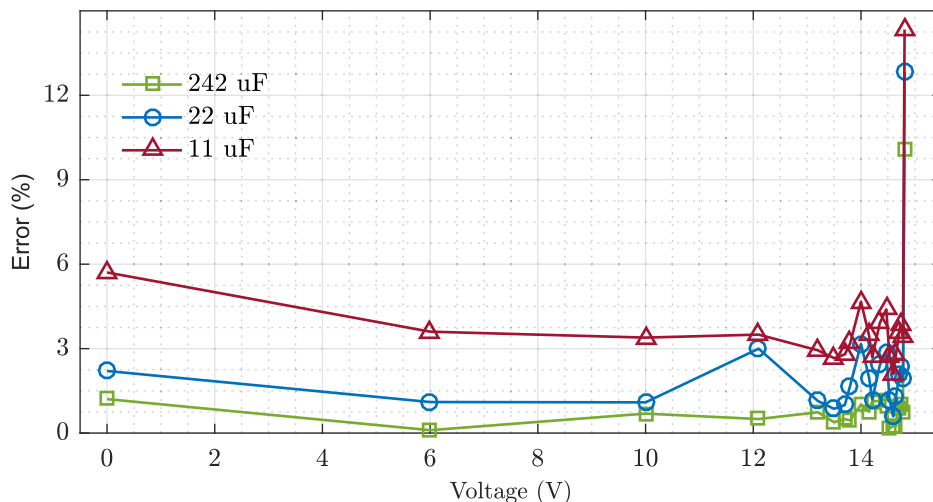

Fig. 15. Error rate (%) between the static and dynamic I-V characteristic for the three capacitor sizes.

For PV modules with high lifetime cells, the hysteresis effect would be even greater. However, previous studies (Ortega et al., 2018) in which parasite capacitances were added to the PV module have shown that from the obtained measurements it is possible to characterize the I-V curve of the PV module.

To quantify the losses of each PV module on large PV systems we propose the use of two parameters: the mismatch and the degradation of the PV module. The mismatch of the PV module is defined as one minus the ratio between the working point and the real maximum power point (MPP). The degradation is defined as one minus the ratio between the real MPP and the expected MPP. These two parameters give a clear indication of the performance of the PV modules and provide information on which specific module is failing. The working point and the real MPP are obtained from the monitoring system. However, to assess the degradation of the module it is necessary to know the expected power, which is obtained from the irradiance level and the operating temperature of the PV cells. In a PV system in which each PV module has an MC connected to it and V_{oc} and I_{sc} are known, it would be possible to statistically estimate the illumination level and the cell temperature for each PV module. For example, if an illumination level of 0.8 suns and a cell temperature of $53\,°C$ were statistically estimated, for a 285 W PV module the expected power would be 202 W. From the measurement data, we could obtain the working point and the real maximum power, which in this example, are 170 W and 195 W respectively. From here, the mismatch of the PV module would be 13% and the degradation would be 3.5%.

6. Conclusions

A novel monitoring methodology has been proposed and evaluated. A prototype of the monitoring circuit has been built and tested.

The proposed monitoring methodology is able to individually evaluate each PV module within a string, without disrupting the normal string operation and without modifying the electrical interconnection circuit.

The monitoring process uses small value capacitors, on the order of tens of microfarads, and low power components. The system has a low cost and a high reliability, since no electrolytic capacitors are used.

The operating point deviations are limited to $\pm0.3\,A$ currents around the operating point. For these currents voltage deviations of approximately 5 V are obtained in less than 5 ms.

From the dynamic I-V characteristics it is possible to estimate the PV module I-V characteristics with accuracies between 1 and 3% for the region close to maximum power and better than 10% for the rest of the I-V curve. The use of higher value capacitors reduces the error, but their higher cost and reduced reliability do not compensate for their use. From these measurement data, it is possible to estimate the PV modules maximum power for medium or high current values with an error below 2%, which increases only to 8.8% when the PV modules is operating with low current values.

Finally, a proposal for failures estimation has been introduced. The methodology is based on giving only two parameters for each PV module - the PV module power losses due to its intrinsic operation - which we have named degradation losses - and the losses for not being at the optimum operating point, which we have named mismatch losses. Using any method that does not disturb the operating point and, from there, estimates the I-V characteristics of the module it sounds hard to distinguish between both parameters.

Acknowledgements

References

Belaout, A., Krim, F., Mellit, A., Talbi, B., Arabi, A., 2018. Multiclass adaptive neuro-fuzzy classifier and feature selection techniques for photovoltaic array fault detection and classification. Renew. Energy 127, 548–558.

Belmili, H., Cheikh, S.M.A., Haddadi, M., Larbes, C., 2010. Design and development of a data acquisition system for photovoltaic modules characterization. Renew. Energy 35, 1484–1492.

Blaesser, G., 1997. PV system measurements and monitoring the European experience. Sol. Energy Mater. Sol. Cells 47, 167–176.

Caron, J.R., Littmann, B., 2013. Direct monitoring of energy lost due to soiling on first solar modules in California. IEEE J. Photovolt. 3, 336–340.

Chouder, A., Silvestre, S., 2010. Automatic supervision and fault detection of PV systems based on power losses analysis. Energy Convers. Manage. 51, 1929–1937.

Cova, P., Delmonte, N., Lazzaroni, M., 2018. Photovoltaic plant maintainability optimization and degradation detection: Modelling and characterization. Microelectron. Reliab. 88, 1077–1082.

Cristaldi, L., Faifer, M., Lazzaroni, M., Khalil, M.M.A.F., Catelani, M., Ciani, L., 2015. Diagnostic architecture: A procedure based on the analysis of the failure causes applied to photovoltaic plants. Measurement 67, 99–107.

Dhimish, M., Holmes, V., 2016. Fault detection algorithm for grid-connected photovoltaic plants. Sol. Energy 137, 236–245.

Drews, A., De Keizer, A., Beyer, H.G., Lorenz, E., Betcke, J., Van Sark, W., Heydenreich, W., Wiemken, E., Stettler, S., Toggweiler, P., et al., 2007. Monitoring and remote failure detection of grid-connected PV systems based on satellite observations. Sol. Energy 81, 548–564.

Duran, E., Galán, J., Sidrach-de Cardona, M., Andujar, J., 2007. A new application of the buck-boost-derived converters to obtain the IV curve of photovoltaic modules. 2007 IEEE Power Electronics Specialists Conference IEEE, 413–417.

Enrique, J., Duran, E., Sidrach-de Cardona, M., Andujar, J., Bohorquez, M., Carretero, J., 2005. A new approach to obtain IV and PV curves of photovoltaic modules by using DC-DC converters. In: Conference Record of the Thirty-first IEEE Photovoltaic Specialists Conference, 2005. IEEE, pp. 1769–1772.

Erkaya, Y., Moses, P., Marsillac, S., 2016. On-site characterization of PV modules using a portable, MOSFET-based capacitive load. In: 2016 IEEE 43rd Photovoltaic Specialists Conference (PVSC). IEEE, pp. 3119–3122.

Firth, S.K., Lomas, K.J., Rees, S.J., 2010. A simple model of PV system performance and its use in fault detection. Sol. Energy 84, 624–635.

Forero, N., Hernández, J., Gordillo, G., 2006. Development of a monitoring system for a PV solar plant. Energy Convers. Manage. 47, 2329–2336.

Fuentes, M., Vivar, M., Burgos, J., Aguilera, J., Vacas, J., 2014. Design of an accurate, low-cost autonomous data logger for PV system monitoring using Arduino? that complies with IEC standards. Sol. Energy Mater. Sol. Cells 130, 529–543.

García, M., Marroyo, L., Lorenzo, E., Marcos, J., Pérez, M., 2014. Observed degradation in photovoltaic plants affected by hot-spots. Prog. Photovoltaics Res. Appl. 22, 1292–1301.

Han, J., Lee, I., Kim, S.H., 2015. User-friendly monitoring system for residential PV system based on low-cost power line communication. IEEE Trans. Consum. Electron. 61, 175–180.

Hoffmann, S., Koehl, M., 2014. Effect of humidity and temperature on the potential-induced degradation. Prog. Photovoltaics Res. Appl. 22, 173–179.

Ibrahim, A., 2011. Analysis of electrical characteristics of photovoltaic single crystal silicon solar cells at outdoor measurements. Smart Grid Renew. Energy 2, 169.

Jäger-Waldau, A., 2019. Snapshot of photovoltaics?february 2019. Energies 12, 769.

Jones, C.B., Ellis, B.H., Stein, J.S., Walters, J., 2018. Comparative review of high resolution monitoring versus standard inverter data acquisition for a single photovoltaic power plant. In: 2018 IEEE 7th World Conference on Photovoltaic Energy Conversion (WCPEC) (A Joint Conference of 45th IEEE PVSC, 28th PVSEC & 34th EU PVSEC). IEEE, pp. 0715–0720.

Kajari-Schršder, S., Kunze, I., Kšntges, M., 2012. Criticality of cracks in PV modules. Energy Procedia 27, 658–663.

Khalid, A.M., Mitra, I., Warmuth, W., Schacht, V., 2016. Performance ratio–crucial parameter for grid connected PV plants. Renew. Sustain. Energy Rev. 65, 1139–1158.

Khatib, T., Elmenreich, W., Mohamed, A., 2017. Simplified IV characteristic tester for photovoltaic modules using a DC-DC boost converter. Sustainability 9, 657.

Kilper, T., Kruse, I., Feser, I., Kirstein, U., Peters, D., 2015. A new generation of PV monitoring system with high-grade remote diagnostic based on module level monitoring and integrated yield simulation. In: 31st European Photovoltaic Solar Energy Conference and Exhibition (EU PVSC 2015), pp. 1679–1682.

Kim, K.A., Krein, P.T., 2013. Hot spotting and second breakdown effects on reverse IV characteristics for mono-crystalline Si photovoltaics. In: 2013 IEEE Energy Conversion Congress and Exposition. IEEE, pp. 1007–1014.

Köntges, M., Kunze, I., Kajari-Schröder, S., Breitenmoser, X., Bjørneklett, B., 2010. Quantifying the risk of power loss in PV modules due to micro cracks. In: 25th European Photovoltaic Solar Energy Conference, Valencia, Spain, pp. 3745–3752.

Kuai, Y., Yuvarajan, S., 2006. An electronic load for testing photovoltaic panels. J. Power Sources 154, 308–313.

Kumar, B.S., Sudhakar, K., 2015. Performance evaluation of 10 MW grid connected solar photovoltaic power plant in india. Energy Reports 1, 184–192.

Mahmoud, M.M., 2006. Transient analysis of a PV power generator charging a capacitor for measurement of the I-V characteristics. Renew. Energy 31, 2198–2206.

Mäki, A., Valkealahti, S., 2012. Power losses in long string and parallel-connected short strings of series-connected silicon-based photovoltaic modules due to partial shading conditions. IEEE Trans. Energy Convers. 27, 173–183.

Mallor, F., León, T., De Boeck, L., Van Gulck, S., Meulders, M., Van der Meerssche, B.,

2017. A method for detecting malfunctions in PV solar panels based on electricity production monitoring. Sol. Energy 153, 51–63.

Matsumoto, Y., Norberto, C., Urbano, J.A., Ortega, M., Asomoza, R., 2016. Three-year PV system performance in Mexico City. In: 2016 IEEE 43rd Photovoltaic Specialists Conference (PVSC). IEEE, pp. 3168–3172.

Morlier, A., Haase, F., Köntges, M., 2015. Impact of cracks in multicrystalline silicon solar cells on PV module power:?a simulation study based on field data. IEEE J. Photovolt. 5, 1735–1741.

Muñoz, J., Lorenzo, E., 2006. Capacitive load based on IGBTs for on-site characterization of PV arrays. Sol. Energy 80, 1489–1497.

Ortega, E., Aranguren, G., Saenz, M., Gutierrez, R., Jimeno, J., 2016. Wireless sensor network for photovoltaic modules monitoring. In: 2016 IEEE 43rd Photovoltaic Specialists Conference (PVSC). IEEE, pp. 2704–2708.

Ortega, E., Aranguren, G., Saenz, M., Gutierrez, R., Jimeno, J., 2017. Study of photovoltaic systems monitoring methods. In: Photovoltaic Specialists Conference (PVSC).

Ortega, E., Aranguren, G., Saenz, M., Gutierrez, R., Jimeno, J., 2018. Photovoltaic module to module monitoring system. In: 2018 IEEE 7th World Conference on Photovoltaic Energy Conversion (WCPEC) (A Joint Conference of 45th IEEE PVSC, 28th PVSEC & 34th EU PVSEC). IEEE, pp. 2703–2708.

Park, N., Jeong, J., Kang, B., Kim, D., 2013. The effect of encapsulant discoloration and delamination on the electrical characteristics of photovoltaic module. Microelectron. Reliab. 53, 1818–1822.

Riley, C., Tolbert, L., 2015. An online autonomousI–V tracer for PV monitoring applications. In: 2015 IEEE Power & Energy Society General Meeting. IEEE, pp. 1–5.

Rivai, A., Rahim, N.A., 2014. Binary-based tracer of photovoltaic array characteristics. IET Renew. Power Gener. 8, 621–628.

Sahbel, A., Hassan, N., Abdelhameed, M.M., Zekry, A., 2013. Experimental performance characterization of photovoltaic modules using DAQ. Energy Procedia 36, 323–332.

Samara, S., Natsheh, E., 2019. Intellingent real-time photovoltaic panel monitoring system using artificial neural networks. IEEE Access 7, 50287–50299.

Sawin, J., et al., 2017. Renewable energy policy network for the 21st century renewables 2017 global status report. REN21 Secretariat: Paris, France, pp. 1–302.

Silvestre, S., Mora-López, L., Kichou, S., Sánchez-Pacheco, F., Dominguez-Pumar, M., 2016. Remote supervision and fault detection on OPC monitored PV systems. Sol. Energy 137, 424–433.

Spertino, F., Ahmad, J., Ciocia, A., Di Leo, P., Murtaza, A.F., Chiaberge, M., 2015. Capacitor charging method for I-V curve tracer and MPPT in photovoltaic systems. Sol. Energy 119, 461–473.

Stein, J.S., McCaslin, S., Hansen, C.W., Boyson, W.E., Robinson, C.D., 2014. Measuring PV system series resistance without full IV curves. In: 2014 IEEE 40th Photovoltaic Specialist Conference (PVSC). IEEE, pp. 2032–2036.

Teubner, J., Kruse, I., Scheuerpflug, H., Buerhop-Lutz, C., Hauch, J., Camus, C., Brabec, C.J., 2017. Comparison of drone-based IR-imaging with module resolved monitoring power data. Energy Procedia 124, 560–566.

Ulasenka, A., Jimeno, J., Obieta, G., Gutierrez, R., Saenz, M., 2015. Module to module monitoring system, M3S, a new strategy for PV-system monitoring. In: 2015 IEEE 42nd Photovoltaic Specialist Conference (PVSC). IEEE, pp. 1–4.

Van Dyk, E., Gxasheka, A., Meyer, E., 2005. Monitoring current–voltage characteristics and energy output of silicon photovoltaic modules. Renew. Energy 30, 399–411.

Vergura, S., Acciani, G., Amoruso, V., Patrono, G.E., Vacca, F., 2009. Descriptive and inferential statistics for supervising and monitoring the operation of PV plants. IEEE Trans. Industr. Electron. 56, 4456–4464.

Wang, J.Y., Qian, Z., Zareipour, H., Wood, D., 2018. Performance assessment of photovoltaic modules based on daily energy generation estimation. Energy 165, 1160–1172.